Toughness of Tempered Upper and Lower Bainitic Microstructures in a 4150 Steel

D.R. Johnson and W.T. Becker

The effects of tempering on the Charpy impact toughness and tensile properties of upper and lower bainite in a 4150 steel have been studied. The results correlate with quantitative measurements taken from both the fracture surfaces and the microstructures of Charpy test specimens. The fracture surfaces from impact specimens having a lower bainitic microstructure were characterized by quasicleavage fracture, whereas those having an upper bainitic microstructure exhibited only cleavage fracture. The quasicleavage facet size and cleavage facet size correlate with bainite packet size and bainite block size. After tempering at high temperatures, the impact toughness is greatly improved for both the upper and lower bainitic microstructures. Changes in toughness correlate with the microstructural change in carbide shape and distribution resulting from the different tempering operations.

Keywords

Charpy impact toughness, bainite microstructure, medium carbon chromium moly steels

1. Introduction

FOR continuous cooling heat treating operations, the optimum combination of strength and toughness is commonly obtained from a properly tempered martensitic microstructure. However, for high-alloy steels having low M_S temperatures and associated large austenite to martensite volume expansions, quench cracking and high residual stresses may result on heat treating. To avoid these problems, a more moderate quenching rate may be desired, sometimes resulting in bainite formation. Such slack-quenched microstructures, where nonmartensitic products are interspersed within a predominantly martensitic matrix, often exhibit a decrease in mechanical properties. Conversely, if the transformation of austenite is done isothermally, fully bainitic microstructures can be produced.

Classically, two distinct bainitic morphologies are identified: upper and lower bainite. Upper bainite consists of ferrite laths with carbide particles at lath boundaries. These carbide particles often have a rod morphology. Lower bainite consists of ferrite plates containing an array of fine spheroidal carbide particles. Slack-quenched materials often contain upper bainite, whereas an austempering heat treatment may be required to produce lower bainite. The toughness of upper bainite is typically considered to be poor, whereas lower bainite may have better toughness values than tempered martensite.[1] It is of interest then to determine if the poor toughness associated with upper bainitic microstructures can be improved with a subsequent tempering operation.

D.R. Johnson and **W.T. Becker,** University of Tennessee, Department of Materials Science and Engineering, Knoxville, Tennessee.

2. Experimental Procedure

Standard full-size Charpy V-notch bars (notched perpendicular to the rolling direction) and half-size tensile bars, having a gage length of 25 mm and a diameter of 6.25 mm, were prepared from a 4150 steel. Heat treatments were performed in two salt bath furnaces, one for austenization and one for the austempering and tempering heat treatments. Test specimens were transferred manually from the high-temperature salt bath to the low-temperature salt bath during the austempering operation. Austenization used a 50% NaCl + 50% KCl salt, whereas a commercial tempering salt was used for the austempering and tempering heat treatments. The heat treating schedule used for the Charpy and tensile bars is schematically shown in Fig. 1. The resulting untempered microstructures have a prior austenite grain size of about 20 μm. A 2% nital solution and a 4% solution of picric acid and methanol were used as etchants. The long tempering times that were used were determined from a previous series of parametric (time, temperature versus hardness) tempering heat treatments.

During the tempering heat treatments, the Charpy bars were wrapped in paper and enclosed in a stainless steel tube (in air) to avoid possible surface reactions with the molten salt. All test specimens were machined before the austempering and tempering heat treatments. Metallographic samples taken from Charpy bars after tempering showed no variation in microstructure from the surface of the bar to the center of the bar. Impact testing was performed using a 360-J Charpy machine using the following test temperatures: –50, 0 (ice bath), 25 (room temperature), 100 (boiling water), and 150 °C. The –50 and 150 °C test temperatures were determined by spot welding a thermocouple to the Charpy bar and heating or cooling to the desired temperature. Three Charpy bars per heat treatment were tested at room temperature. Two bars per heat treatment were used for the other test temperatures. Tensile tests were conducted on a screw-driven frame at a crosshead speed of 0.25 mm/min.

Average Vickers hardness measurements with a standard deviation less than ±15 DPH were obtained using at least ten hardness measurements. Hardness measurements were taken at 1-kg load with a dwell time of 15 s.

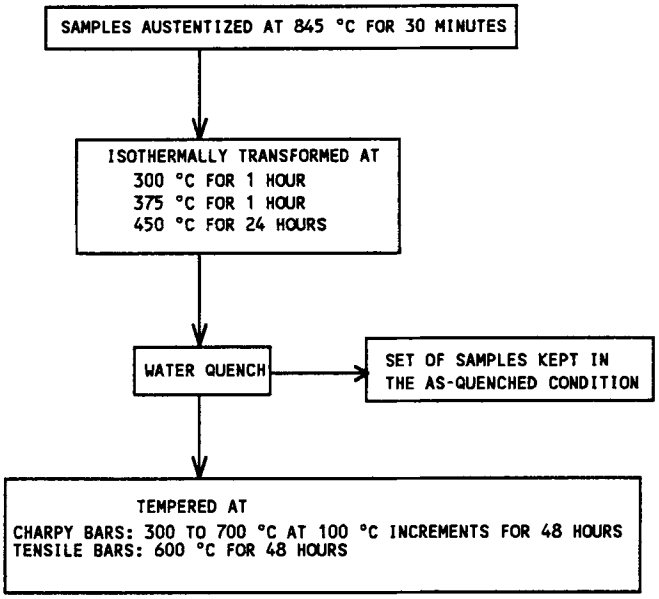

Fig. 1 Heat treating schedule for both Charpy and tensile test specimens.

3. Microstructures

The starting upper and lower bainite morphologies were chosen from a set of partially transformed samples, because the bainite morphology can be distinguished more readily. These microstructures are shown in Fig. 2. Austempering at 300 and 375 °C produced lower bainitic microstructures that were identified by the fine distribution of carbides within the bainitic ferrite plates. Austempering at 450 °C produced an upper bainitic microstructure. The irregular shapes produced by the upper bainite "feather" on the polished surface are coarse enough to distinguish them from lower bainite. These transformation temperatures were then used to obtain the fully bainitic microstructures of the test specimens.

To compare the isothermally transformed microstructures to the tempered microstructures, the average carbide spacing and the maximum carbide length (for those having a large aspect ratio) were measured for each heat treatment. The linear intercept method was used to find the average carbide spacing. The maximum carbide length was found from the average of the five largest carbide measurements taken from each photomicrograph. Measurements were taken from a total of 25 scanning electron microscope (SEM) photomicrographs, with the results shown in Table 1. The different bainitic microstructures and those tempered at 600 °C are shown in Fig. 3.

Note that increasing the transformation temperature greatly increases the maximum carbide length. For example, the 450 °C transformed microstructure has the greatest average carbide spacing and the greatest maximum carbide length. However, tempering produces little change in the carbide morphology for all of these microstructures until a tempering temperature near 600 °C is reached. Unlike martensite, which is supersaturated in carbon with respect to the equilibrium phase ferrite, the amount of carbide precipitation expected from tempering bainite is small, if any. Only spheroidization and coarsening are expected. Hence, only tempering temperatures near-

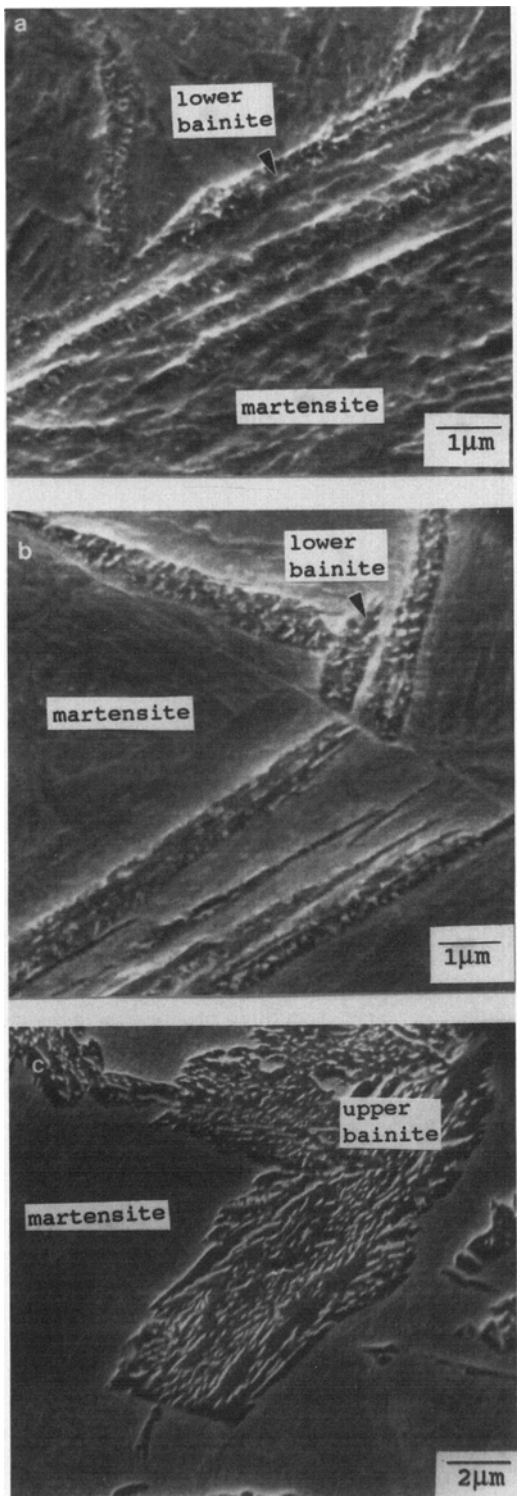

Fig. 2 SEM photographs of partially transformed bainitic microstructures. (a) Isothermally transformed at 300 °C for 1 min. (b) Isothermally transformed at 375 °C for 1 min. (c) Isothermally transformed at 450 °C for 1 min.

ing the eutectoid temperature will produce large changes in the carbide morphology.

Microstructural change first occurs for tempering temperatures near 600 °C. At this temperature, carbides with a high aspect ratio begin to spheroidize and the average carbide spacing decreases as the long carbide particles pinch-off into many smaller ones. This process occurs in both the 375 and 450 °C transformed microstructures. Because the carbides in the 300 °C transformed microstructure are already spheroidal, only coarsening occurs at this temperature, increasing the average carbide spacing. Tempering at 700 °C causes the average carbide spacing to increase in all of the microstructures due to Ostwald ripening. After such a tempering heat treatment, the different bainitic microstructures have similar values for the average carbide spacing and the maximum carbide length as an equilibrium configuration is approached.

4. Mechanical Properties

Charpy curves for each bainite morphology were determined for the untempered microstructure and for those tempered at 500 and 600 °C. These results are shown in Fig. 4. An estimation of the transition temperature for each Charpy curve, the corresponding upper shelf impact energy values, and the average hardness values are listed in Table 2. Percentage shear measurements were used to estimate a 50% fracture appearance transition temperature (FATT) for the different curves. Charpy specimens having a 100% shear fracture surface were considered to lay on the upper shelf of the Charpy curve. Comparing the Charpy curves reveals that similar upper shelf values are obtained for all three morphologies after tempering at 600 °C. However, the upper bainitic specimens still have a higher transition temperature.

Tensile properties were determined for the low- and high-toughness conditions for the different bainite morphologies. The results are listed in Table 3. In the untempered condition, the tensile strength of the upper bainitic specimen is significantly less than those having a lower bainitic microstructure. In addition, the upper bainitic specimen has the greater percentage of tensile elongation. However, after tempering at 600 °C, similar tensile properties are measured for both the upper and lower bainitic specimens. A yield point effect with accompanying Lüders strain was observed for these tempered specimens.

Table 1 Average carbide spacing and maximum carbide length for various bainitic microstructures

Condition	Average carbide spacing, μm	Maximum carbide length, μm
Isothermally transformed at 300 °C	0.20 ± 0.05	0.33 ± 0.11
Tempered at 400 °C	0.17 ± 0.03	0.44 ± 0.15
Tempered at 500 °C	0.15 ± 0.03	0.39 ± 0.10
Tempered at 600 °C	0.32 ± 0.09	(round)
Isothermally transformed at 375 °C	0.16 ± 0.05	1.0 ± 0.24
Tempered at 400 °C	0.21 ± 0.06	0.99 ± 0.16
Tempered at 500 °C	0.28 ± 0.07	0.89 ± 0.12
Tempered at 600 °C	0.22 ± 0.04	0.54 ± 0.26
Tempered at 700 °C	0.37 ± 0.08	0.46 ± 0.06
Isothermally transformed at 450 °C	0.30 ± 0.10	2.7 ± 0.65
Tempered at 400 °C	0.29 ± 0.07	2.2 ± 0.45
Tempered at 500 °C	0.33 ± 0.07	2.3 ± 0.45
Tempered at 600 °C	0.24 ± 0.06	1.4 ± 0.42
Tempered at 700 °C	0.37 ± 0.04	0.86 ± 0.16

Note: Tempering time was 48 h.

5. Fracture Characteristics

Before considering the potential fracture characteristics of the tempered bainitic microstructures, the macroscopic failure surfaces from the Charpy test specimens should first be examined. If fracture occurs at inclusion/matrix interfaces, then the observed differences in microstructure due to tempering may have little influence on the measured toughness.

Table 2 Results from Charpy impact tests for various bainitic microstructures

Condition	50% FATT, °C	Charpy upper shelf, J	Hardness, DPH
Isothermally transformed at 300 °C	>150	...	531
Tempered at 500 °C	25	88	345
Tempered at 600 °C	–60	118	285
Isothermally transformed at 375 °C	115	61	394
Tempered at 500 °C	70	100	330
Tempered at 600 °C	–30	125	258
Isothermally transformed at 450 °C	130	...	301
Tempered at 500 °C	100	75	293
Tempered at 600 °C	25	115	248

Table 3 Results from tensile tests for various bainitic microstructures

Condition	Ultimate tensile strength, MPa	Yield strength, MPa	Elongation, %	Reduction of area, %
Isothermally transformed at 300 °C	1720	1590	12.5	48.7
Tempered at 600 °C	830	730	25.0	66.4
Isothermally transformed at 375 °C	1320	1170	15.6	59.0
Tempered at 600 °C	790	650	25.0	66.8
Isothermally transformed at 450 °C	970	810	18.8	48.7
Tempered at 600 °C	730	530	25.0	64.0

Figure 5 shows the representative cross sections of two fracture surfaces taken from Charpy bars broken in low- and high-toughness conditions. The initial mode of fracture is ductile, as indicated by a 45° shear lip below the notch root. The fracture then proceeds in an opening mode perpendicular to the sulfide inclusions. Examining the fracture surface more closely reveals that the propagating crack does follow the sulfide inclusions over short distances, resulting in occasional "steps" in the fracture profile. The presence of the sulfide inclusions is more visible in the microstructure tempered to a high-toughness con-

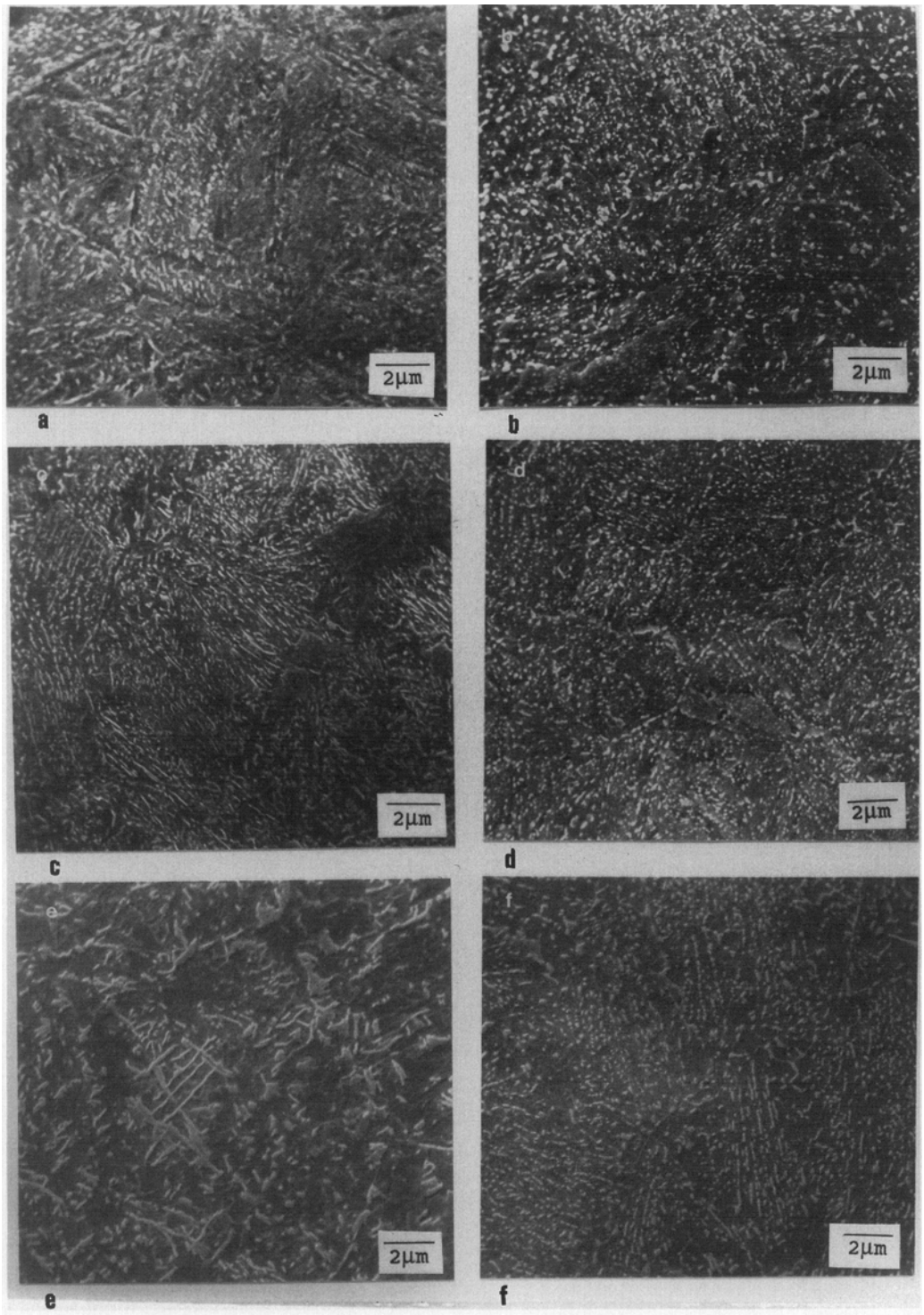

Fig. 3 SEM photographs of isothermally transformed and tempered bainitic microstructures. (a) Isothermally transformed at 300 °C, 1 h; then (b) tempered at 600 °C for 48 h. (c) Isothermally transformed at 375 °C, 1h; then (d) tempered at 600 °C for 48 h. (e) Isothermally transformed at 450 °C, 24 h; then (f) tempered at 600 °C for 48 h.

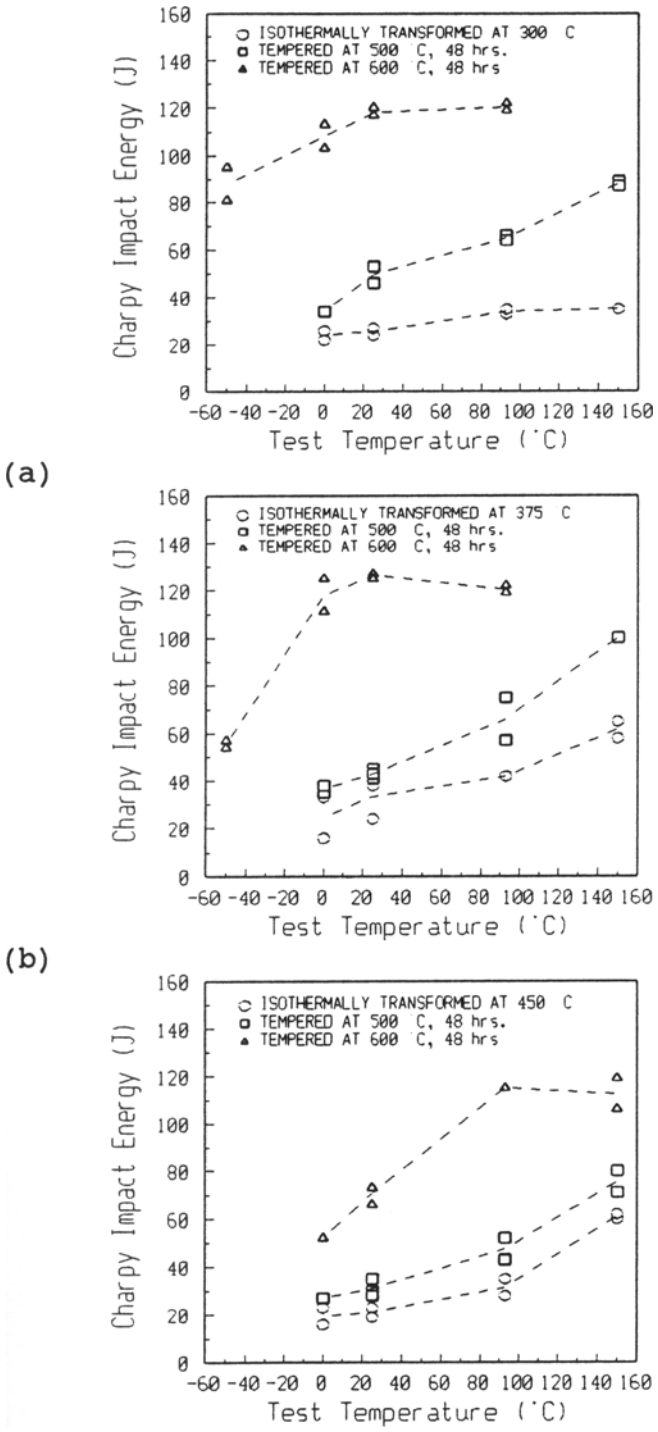

Fig. 4 Results from Charpy impact tests. Isothermally transformed at (a) 300 °C, (b) 375 °C, and (c) 450 °C and subsequently tempered at 500 and 600 °C.

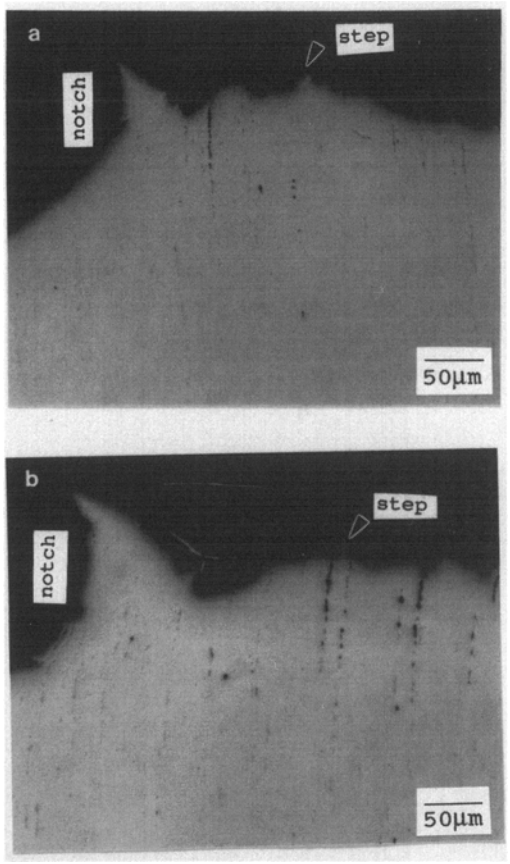

Fig. 5 Optical photomicrographs taken at the root of Charpy impact specimens broken at room temperature. Unetched. (a) Low-toughness condition. Isothermally transformed at 375 °C, 1 h, then tempered at 500 °C, 48 h. (b) High-toughness condition. Isothermally transformed at 375 °C, 1 h, then tempered at 600 °C, 48 h.

dition due to the large voids that nucleate around the inclusions during dimpled fracture. However, the spacing between the sulfide inclusions is large compared to either the prior austenite grain size or the carbide spacing. Therefore, the majority of the fracture processes are characteristic of the bainitic microstructure.

Typical fracture surfaces of Charpy impact specimens broken below their ductile-brittle transition temperature (DBTT) are shown in Fig. 6. Impact specimens having lower bainitic microstructures are characterized by a quasicleavage fracture surface. Upper bainitic impact specimens exhibit only a cleavage fracture surface. After tempering at 600 °C, impact toughness is greatly improved for both the upper and lower bainitic Charpy specimens. These tempered specimens have a dimpled fracture surface, as shown in Fig. 7.

From the fracture surfaces of the lower bainitic Charpy specimens broken below their DBTT, there are three measurable features: the quasicleavage facet size (a set of cleavage facets surrounded by tear marks), the cleavage facet size, and the regions of fracture associated with prior austenite grain boundaries. Only cleavage fracture is observed for the upper bainitic Charpy specimens. All of these features can be measured and compared to measurable features in the corresponding microstructure.

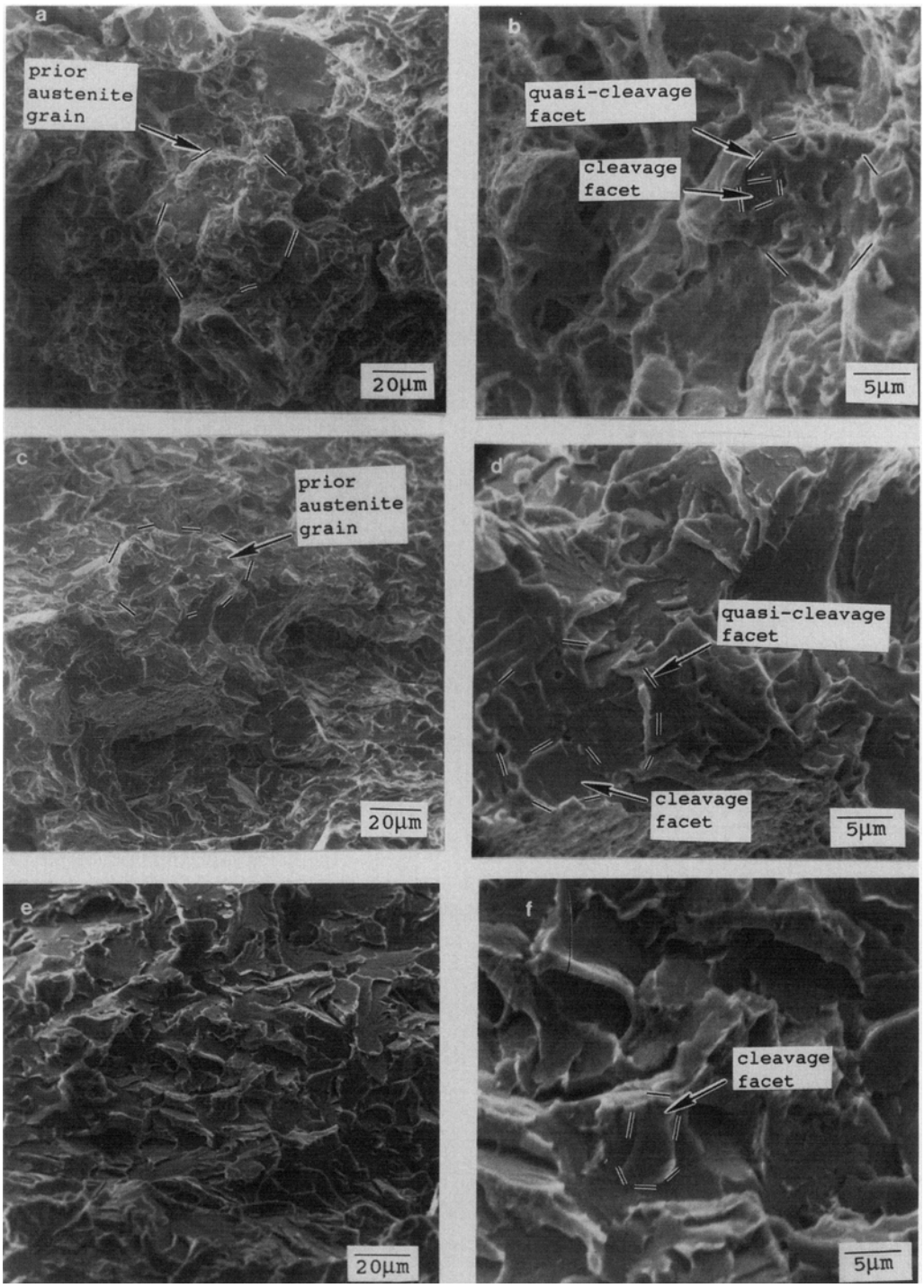

Fig. 6 Typical SEM photographs of fracture surfaces for bainitic impact specimens broken below their DBTT. (a) and (b) isothermally transformed at 300 °C, 1h. (c) and (d) isothermally transformed at 375 °C, 1h. (e) and (f) isothermally transformed at 450 °C, 24 h.

From optical and SEM photomicrographs, the following features were measured: the prior austenite grain size, the bainite packet size, and the bainite block size. The bainite packet and bainite block size are defined in Fig. 8. The bainite packet size is a group of parallel laths or plates that partition the prior austenite grains. Smaller groups of laths may partition the packets into blocks.[2] High-angle boundaries may separate these packets and blocks from one another, whereas low-angle boundaries separate the individual laths and plates.[3,4]

Packet and block sizes did not change for tempering temperatures below 700 °C. Thus, an average packet and average block size were calculated for each bainite morphology. These

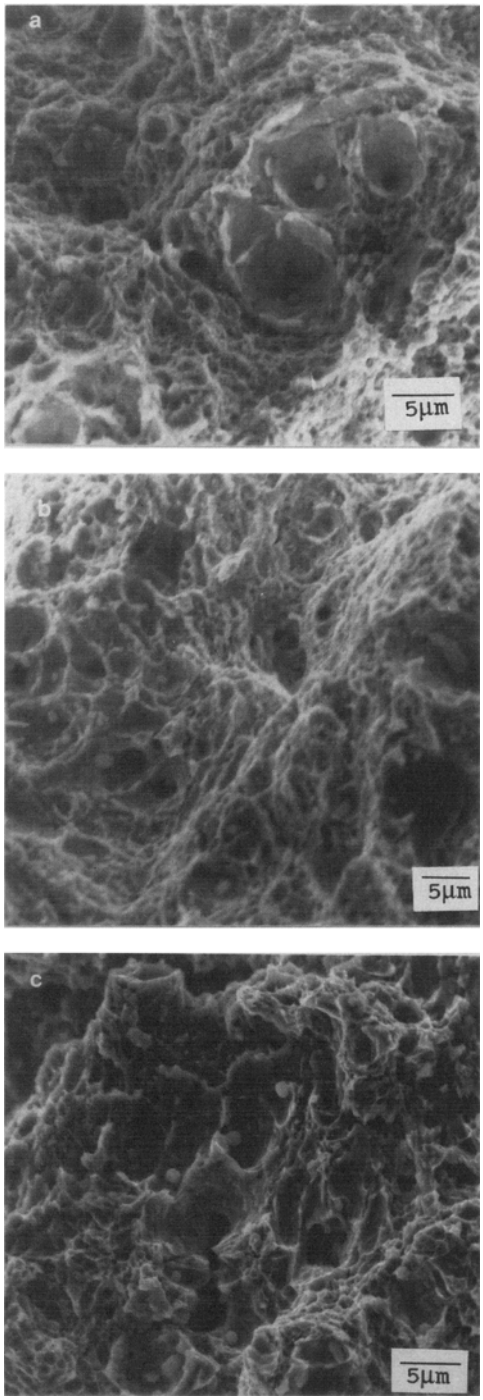

Fig. 7 Typical SEM photographs of fracture surfaces of bainitic impact specimens broken above their DBTT. (a) Isothermally transformed at 300 °C, 1 h, then tempered at 600 °C, 48 h. (b) Isothermally transformed at 375 °C, 1h, then tempered at 600 °C, 48 h. (c) Isothermally transformed at 450 °C, 24 h, then tempered at 600 °C, 48 h.

measurements were then compared to the measurements taken from the fracture surfaces and are listed in Table 4. All measurements have a standard deviation less than 1 μm, except the prior austenite grain size measurements which are closer to ±4 μm.

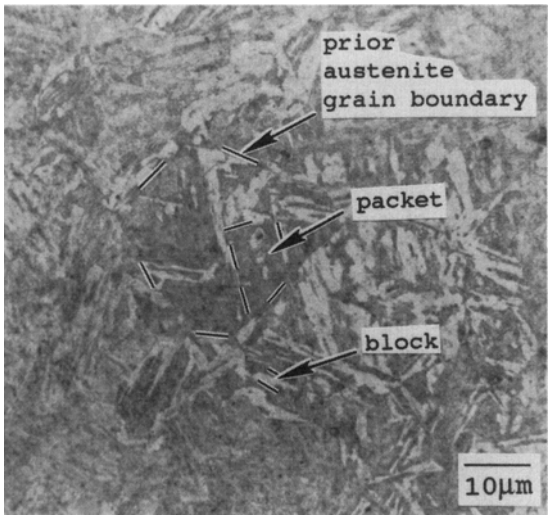

Fig. 8 Optical photomicrograph of a bainitic microstructure transformed at 375 °C showing packets and blocks within a prior austenite grain.

The prior austenite grain size measured from the fracture surfaces (about 19 ± 4 μm) corresponds quite well with those measured from the microstructures using optical microscopy (20 ± 3 μm). Similarly, the block size and packet size correspond to the cleavage facet size and the quasicleavage facet size. Measurements taken from the fracture surfaces are consistently larger than those taken from the microstructures. This has been reported to result from a continuation of cleavage planes for similarly oriented bainite packets or blocks.[5]

To find how a crack may nucleate and propagate through the different microstructures, metallographic samples were taken through the fracture surfaces of broken Charpy bars. The different fracture modes observed in the lower bainitic microstructures are shown in Fig. 9. In the low-toughness condition, the high-angle packet and block boundaries or prior austenite grain boundaries may either arrest crack propagation or cause a change in crack direction. In contrast, low-angle block boundaries within a packet may change the crack direction by only small angles. Finally, in the tougher conditions, voids form around the sulfide inclusions and around the carbides, with failure initiated by void coalescence.

The different fracture modes observed in the upper bainitic microstructures are shown in Fig. 10. The microcracks in the upper bainitic microstructures are very smooth cleavage cracks whose propagation seem oblivious to the presence of the large carbides. Observation of the microstructure at the root of the Charpy notch shows that both debonding along the carbide/ferrite interfaces and carbide cracking are present. These larger carbides act as starter cracks, decreasing the toughness of the upper bainitic microstructure. Tempering the upper bainitic microstructure at 600 °C and above reduces the aspect ratio of the large carbides and produces a change in the fracture mode from cleavage to void coalescence, which results in improved toughness.

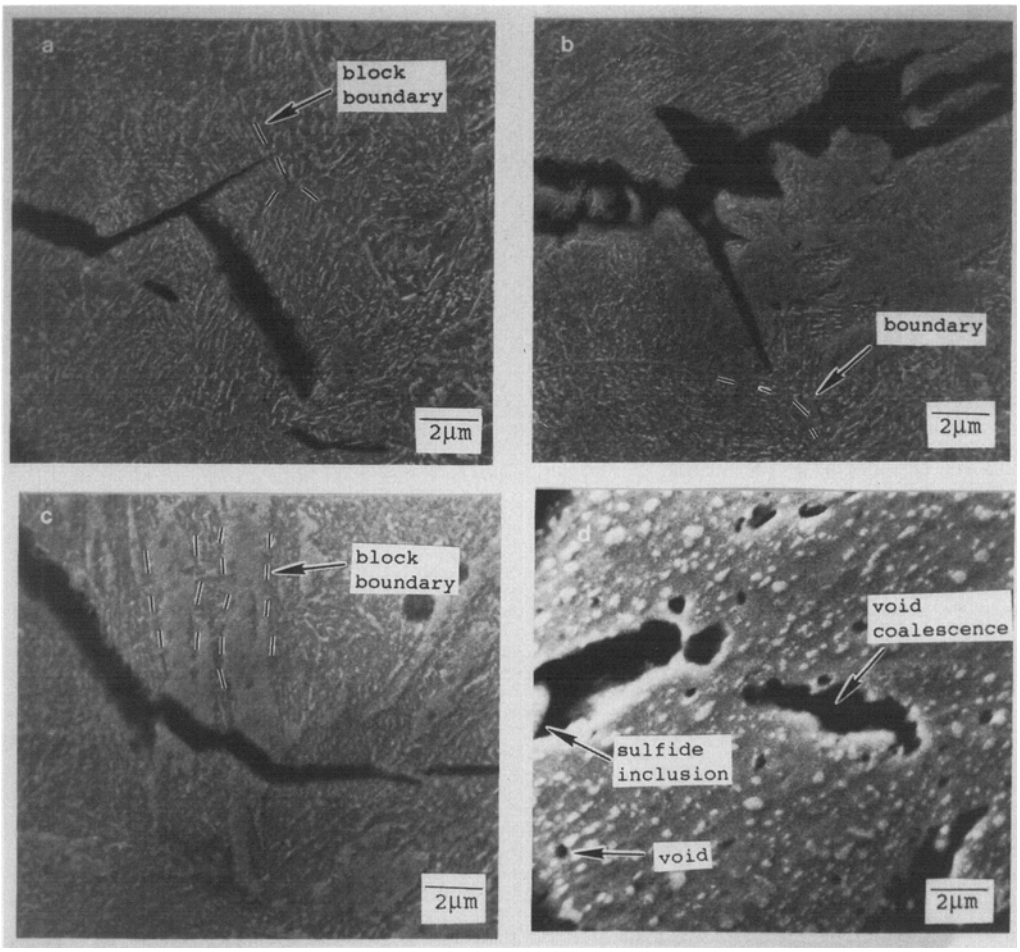

Fig. 9 SEM photographs of different fracture modes observed in lower bainitic microstructures. (a) Effect of high-angle boundaries on cleavage crack propagation. Transformation at 375 °C. (b) Effect of high-angle boundaries on cleavage crack propagation. Transformation at 375 °C. (c) Effect of low-angle boundaries on cleavage crack propagation. Transformation at 375 °C. (d) Fracture initiation by void coalescence. Transformation at 300 °C. Tempered at 600 °C.

Table 4 Packet size and block size determined from both SEM and optical photomicrographs (OM) compared to features measured on the fracture surfaces

Isothermal transformation temperature, °C	Block size, μm		Packet size (OM), μm	Facet size, μm	Quasi-cleavage size, μm	Prior austenite grain size (fracture surface), μm
	OM	SEM				
300	2.4	1.7	4.6	2.5	6.8	18.8
375	2.2	2.4	4.9	2.6	5.7	18.0
450	3.2	3.4	...	5.2	...	19.3

6. Conclusions

In the low-toughness condition, the high-angle bainite packet boundaries can affect the propagation of a cleavage crack. Tempering the different microstructures to temperatures up to 600 °C produces little change in the bainite packet size or the bainite block size. Hence, any change in toughness from tempering is not due to a change in the distance between the high-angle packet boundaries.

The changes in carbide shape and distribution are the most notable differences observed in the untempered and tempered microstructures. For the untempered bainitic microstructures, the much larger carbides of the upper bainite morphologies are responsible for their lower toughness by providing sites for crack nucleation. For upper bainite, crack nucleation occurs by both carbide cracking and debonding along the carbide/ferrite interface. Upon tempering at 600 °C, the Charpy upper shelf values and also the tensile properties approach similar levels for the different bainitic microstructures. In addition, the carbide shape and spacing for the different bainitic microstructures also approach similar values after tempering. Hence, the toughness of the upper bainite can be directly correlated to the shape and distribution of the carbide particles.

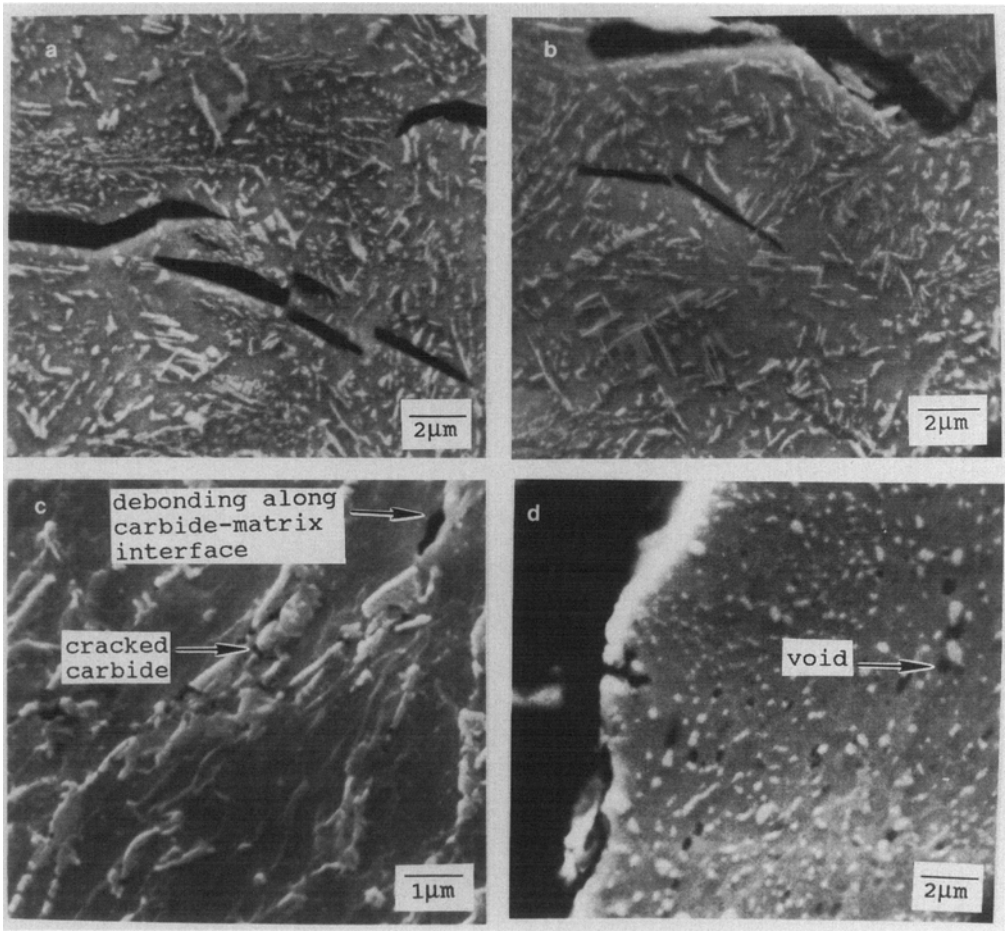

Fig. 10 SEM photographs of different fracture modes observed in upper bainitic microstructures. Transformation at 450 °C, 24 h. (a) Cleavage cracks in an upper bainitic microstructure. (b) Cleavage cracks in an upper bainitic microstructure. (c) Upper bainitic microstructure at the root of a Charpy notch showing carbide cracking and debonding along carbide/matrix interfaces. (d) Fracture initiation by void coalescence. Tempered at 700 °C, 48 h.

Finally, the toughness of upper bainite can be improved by tempering at high temperatures. After such a tempering heat treatment, both upper and lower bainite have similar Charpy upper shelf values and similar tensile strengths. However, the tensile strength of the lower bainitic microstructure is nearly halved. Thus, the poor toughness associated with upper bainite in a slack-quenched microstructure may be minimized by a tempering heat treatment if the resulting loss in strength can be tolerated.

Acknowledgment

Appreciation is extended to Dr. C.R. Brooks, Rob Reviere, and Steve Joslin for their helpful discussions.

References

1. R.F. Hehemann, V.J. Luhan, and A.R. Troiano, The Influence of Bainite on Mechanical Properties, *Trans. ASM*, Vol 49, 1957, p 409-426
2. Y. Tomita and K. Okabayashi, Effect of Microstructure on Strength and Toughness of Heat Treated Low Alloy Structural Steels, *Metall. Trans. A*, Vol 17, 1986, p 1203-1209
3. A.R. Marder and G. Krauss, The Morphology of Martensite Iron-Carbon Alloys, *Trans. ASM*, Vol 60, 1967, p 651-660
4. J.M. Marder and A.R. Marder, The Morphology of Iron-Nickel Massive Martensite, *Trans. ASM*, Vol 62, 1969, p 1-10
5. Y. Ohmori, H. Ohtani, and T. Kunitake, Tempering of the Bainite and the Bainite/Martensite Duplex Structure in Low Carbon Low-Alloy Steel, *Met. Sci.*, Vol 8, 1974, p 357-366